International Journal of Control, Automation and Systems 15(5) (2017) 2013-2025
http://dx.doi.org/10.1007/s12555-016-0589-2

ISSN:1598-6446 eISSN:2005-4092
http://www.springer.com/12555

# Interacting Multiple Model Estimation-based Adaptive Robust Unscented Kalman Filter

**Bingbing Gao*, Shesheng Gao, Yongmin Zhong, Gaoge Hu, and Chengfan Gu**

**Abstract:** The unscented Kalman filter (UKF) is a promising approach for the state estimation of nonlinear dynamic systems due to its simple calculation process and superior performance in highly nonlinear systems. However, its solution will be degraded or even divergent when the system model involves uncertainty. This paper presents an interacting multiple model (IMM) estimation-based adaptive robust UKF to address this problem. This method combines the merits of the adaptive fading UKF and robust UKF and discards their demerits to inhibit the disturbance of system model uncertainty on the filtering solution. An adaptive fading UKF for the case of process model uncertainty and a robust UKF for the case of measurement model uncertainty are established based on the principle of innovation orthogonality. Subsequently, an IMM estimation is developed to fuse the adaptive fading UKF and robust UKF as sub-filters according to the mode probability. The system state estimation is achieved as a probabilistic weighted sum of the estimation results from the two sub-filters. Simulations, experiments and comparison analysis validate the efficacy of the proposed method.

**Keywords:** Adaptive fading factor, interacting multiple model, robust factor, system model uncertainty, unscented Kalman filter.

## 1. INTRODUCTION

The problem of state estimation in nonlinear dynamic systems has been attracted considerable research interests during the past several decades since it has widespread applications in numerous science and engineering fields such as vehicle navigation, signal processing, radar tracking, and automatic control [1–4]. The extended Kalman filter (EKF), which is a nonlinear version of Kalman filter, is the most commonly used filtering approach for nonlinear systems [5,6]. The unscented Kalman filter (UKF) is a relatively new nonlinear filtering method which has many advantages over the EKF [7–9]. Given the fact that it is much easier to approximate a probability distribution than any other nonlinear transformation, the UKF directly uses unscented transformation to approximate the probability density of state distribution, overcoming the linearization error involved in the EKF. Therefore, the UKF can approximate the posterior mean and covariance of any Gaussian random variable in third-order accuracy, whereas the EKF in first-order accuracy. Furthermore, the UKF does not require the computation of Jacobian matrices and has the merits such as the simplicity in implementation, high estimation accuracy and high convergence rate [9, 10]. Given these merits, the UKF has become a promising solution to address the problem of nonlinear state estimation [10–12].

However, the UKF requires an accurate system model and exact noise statistics information [13,14]. It is difficult to satisfy these conditions in practice. The system model usually involves uncertainties such as the model parameter mismatch, system noise statistic error and stochastic drifts, leading to the deteriorated or even divergent UKF solution [15, 16].

This paper presents an interacting multiple model estimation-based adaptive robust UKF (IMM-ARUKF) to overcome the problem of the classical UKF in requirement of accurate system model and exact noise statistics information. Based on the principle of innovation orthogonality, this method establishes an adaptive fading UKF (AFUKF) for the case of process model uncertainty and a robust UKF (RUKF) for the case of measurement model uncertainty. Subsequently, it further develops an interacting multiple model estimation to fuse the AFUKF and RUKF according to the mode probability calculated from the innovation information of both filters to combine their advantages and eliminate their limitations. The overall system state estimation is obtained as the probabilistic weighted sum of the estimation results from the two fil-

Manuscript received September 20, 2016; accepted December 20, 2016. Recommended by Associate Editor Yingmin Jia under the direction of Editor Duk-Sun Shim. The work of this paper was supported by the National Natural Science Foundation of China (Project Number: 61174193) and the Specialized Research Fund for the Doctoral Program of Higher Education (Project Number: 20136102110036).

Bingbing Gao, Shesheng Gao, and Gaoge Hu are with the School of Automatics, Northwestern Polytechnical University, Xian 710072, China (e-mails: nwpugbb0826@126.com, gshshnpu@163.com, hugaoge1111@126.com). Yongmin Zhong and Chengfan Gu are with the School of Engineering, RMIT University, Bundoora, VIC 3083, Australia (e-mails: yongmin.zhong@rmit.edu.au, chengfan.gu@rmit.edu.au).
* Corresponding author.


©ICROS, KIEE and Springer 2017

ters. The proposed IMM-ARUKF not only overcomes the limitation of the classical UKF in requirement of accurate system model, but it also absorbs the merits and discards the demerits of the AFUKF and RUKF, leading to improved adaptability and robustness. Simulations, practical experiments and comparison analysis have been conducted to comprehensively evaluate the performance of the proposed IMM-ARUKF.

## 2. RELATED WORK

Research efforts have been dedicated to improvement of the UKF adaptability and robustness against system model uncertainty. Cho and Choi presented a sigma-point based receding horizon Kalman filter (SPRHKF) to improve the UKF robustness [17]. This method uses a receding horizon strategy to adaptively resist model errors and temporarily unknown sensor bias. However, since this filter is based on a finite impulse response structure, its filtering convergence is poor [18]. Song and Han studied a method to improve the UKF performance against process model uncertainty by minimizing the difference between the estimated covariance and actual innovation covariance [19]. However, this method requires the calculation of partial derivatives, leading to a relatively large computational burden [14]. Jwo et al. used fuzzy logic to detect model uncertainties for improvement of the UKF adaptability and robustness [20, 21]. However, the fuzzy rules are developed based on empiricism and heuristic information, leading to the limited performance.

Studies have also reported focusing on the use of the scaling factor to improve the UKF adaptability and robustness. These studies can be divided into two categories. One is the AFUKF. Under the assumption that the actual measurement is accurate, the AFUKF scales the process noise covariance or predicted state covariance using the adaptive fading factor to compensate process model uncertainty [14, 15]. The other is the RUKF, which the exact opposite of the AFUKF. The RUKF scales the measurement noise covariance or innovation covariance with a robust factor to deal with the measurement model uncertainty under the assumption that the process model is constructed correctly [22, 23]. Both methods have their own merits. The AFUKF can strongly track the discontinuous variation of system state, while the RUKF is insensitive to abnormal measurement. As these two filters have complementary features with each other, an obvious solution is to combine them together to handle both process and measurement model uncertainties. However, as the AFUKF cannot handle measurement model uncertainty and the RUKF cannot handle process model uncertainty, a simple combination of both filters to handle process model uncertainty and measurement model uncertainty would deteriorate the filtering solution [24]. Therefore, it is necessary to study how to effectively combine both filters together to fully take their individual advantages for improvement of the UKF adaptability and robustness.

The interacting multiple model (IMM) estimation has received a great deal of attention in the recent years due to its great success in handling multi-mode behavior problems in the areas of target tracking, fault detection and fault isolation [25–28]. This method runs several sub-filters in parallel, each matching a particular system mode. The probability of each mode is characterized using a likelihood function, and the transition between system modes is performed via a transition probability. The overall state estimation is computed as a probabilistically weighted sum of the results from each sub-filter. According to the mode probability calculated from the innovation information of individual sub-filters, the IMM can always follow a sub-filter that outperforms others. Therefore, the IMM is very suitable for integration of the AFUKF and RUKF to make full use of their respective merits and diminish their demerits. However, there has been very limited research on using the IMM to combine AFUKF and RUKF to improve the UKF performance.

This paper presents a new IMM-ARUKF to address the problem of the classical UKF in requirement of accurate system model. The novelty of the paper is that the IMM estimation is established for fusion of the AFUKF and RUKF to combine their advantages and eliminate their limitations, thus improving the UKF adaptability and robustness in presence of system model uncertainty.

## 3. CLASSICAL UKF

Consider the nonlinear dynamic system with additive noises as follows:

$$\begin{cases} \boldsymbol{x}_k = f(\boldsymbol{x}_{k-1}) + \boldsymbol{w}_k, \\ \boldsymbol{z}_k = h(\boldsymbol{x}_k) + \boldsymbol{v}_k, \end{cases} \tag{1}$$

where $\boldsymbol{x}_k \in \mathbf{R}^n$ and $\boldsymbol{z}_k \in \mathbf{R}^m$ are the state vector and measurement vector at time $k$; $f(\cdot)$ and $h(\cdot)$ are the nonlinear functions describing the process and measurement models; and $\boldsymbol{w}_k \in \mathbf{R}^n$ and $\boldsymbol{v}_k \in \mathbf{R}^m$ are the process and measurement noises, which are assumed as uncorrelated zero-mean Gaussian white noises with covariances

$$E\left[\boldsymbol{w}_k \boldsymbol{w}_j^{\mathrm{T}}\right] = \boldsymbol{Q}_k \delta_{kj}, \;\; E\left[\boldsymbol{v}_k \boldsymbol{v}_j^{\mathrm{T}}\right] = \boldsymbol{R}_k \delta_{kj}, \tag{2}$$

where $\boldsymbol{Q}_k$ is a non-negative definite matrix, $\boldsymbol{R}_k$ is a positive definite matrix, and $\delta_{kj}$ is the *Kronecker-*$\delta$ function.

The computational process of the classical UKF for the nonlinear system described by (1) can be summarized as:

**Step 1:** *Initialization.*

$$\begin{cases} \hat{\boldsymbol{x}}_0 = \mathrm{E}[\boldsymbol{x}_0], \\ \boldsymbol{P}_0 = \mathrm{E}\left[(\boldsymbol{x}_0 - \hat{\boldsymbol{x}}_0)(\boldsymbol{x}_0 - \hat{\boldsymbol{x}}_0)^{\mathrm{T}}\right]. \end{cases} \tag{3}$$

**Step 2:** *Time Update.* Given the state estimate $\hat{\boldsymbol{x}}_{k-1}$ and its error covariance matrix $\boldsymbol{P}_{k-1}$, the sigma points can be selected by

$$\begin{cases} \boldsymbol{\chi}_{i,k-1} = \hat{\boldsymbol{x}}_{k-1}, & i=0, \\ \boldsymbol{\chi}_{i,k-1} = \hat{\boldsymbol{x}}_{k-1} + \left(a\sqrt{n\boldsymbol{P}_{k-1}}\right)_i & i=1,2,\cdots,n, \\ \boldsymbol{\chi}_{i,k-1} = \hat{\boldsymbol{x}}_{k-1} - \left(a\sqrt{n\boldsymbol{P}_{k-1}}\right)_{i-n}, & i=n+1,n+2,\cdots,2n, \end{cases} \tag{4}$$

where $a$ is the tuning parameter that determines the spread of the sigma points around $\hat{\boldsymbol{x}}_{k-1}$, and it is usually set to a small positive value; and $\left(\sqrt{n\boldsymbol{P}_{k-1}}\right)_i$ denotes the $i$th column of the square root of the matrix $n\boldsymbol{P}_{k-1}$.

The sigma points are instantiated through the process model to yield a set of transformed samples

$$\boldsymbol{\chi}_{i,k/k-1} = f(\boldsymbol{\chi}_{i,k-1}), \quad i=0,1,\cdots,2n. \tag{5}$$

The predicted state mean and covariance are calculated as

$$\hat{\boldsymbol{x}}_{k/k-1} = \sum_{i=0}^{2n} \omega_i \boldsymbol{\chi}_{i,k/k-1} = \sum_{i=0}^{2n} \omega_i f(\boldsymbol{\chi}_{i,k-1}), \tag{6}$$

$$\boldsymbol{P}_{k/k-1} = \sum_{i=0}^{2n} \omega_i (\boldsymbol{\chi}_{i,k/k-1} - \hat{\boldsymbol{x}}_{k/k-1})(\boldsymbol{\chi}_{i,k/k-1} - \hat{\boldsymbol{x}}_{k/k-1})^{\mathrm{T}} + \boldsymbol{Q}_k, \tag{7}$$

where $\begin{cases} \omega_i = 1 - \dfrac{1}{a^2}, & i=0, \\ \omega_i = \dfrac{1}{2na^2}, & i=1,2,\cdots,2n \end{cases}$.

**Step 3:** *Sigma Point Update.* A set of new sigma points is reselected with the mean $\hat{\boldsymbol{x}}_{k/k-1}$ and the covariance $\boldsymbol{P}_{k/k-1}$

$$\begin{cases} \boldsymbol{\chi}'_{i,k/k-1} = \hat{\boldsymbol{x}}_{k/k-1}, & i=0, \\ \boldsymbol{\chi}'_{i,k/k-1} = \hat{\boldsymbol{x}}_{k/k-1} + \left(a\sqrt{n\boldsymbol{P}_{k/k-1}}\right)_i, & i=1,2,\cdots,n, \\ \boldsymbol{\chi}'_{i,k/k-1} = \hat{\boldsymbol{x}}_{k/k-1} - \left(a\sqrt{n\boldsymbol{P}_{k/k-1}}\right)_{i-n}, & \\ & i=n+1,n+2,\cdots,2n. \end{cases} \tag{8}$$

**Step 4:** *Measurement Update.* The transformed sigma points for measurement are

$$\boldsymbol{\gamma}_{i,k/k-1} = h(\boldsymbol{\chi}'_{i,k/k-1}). \tag{9}$$

The predicted measurement is calculated by

$$\hat{\boldsymbol{z}}_{k/k-1} = \sum_{i=0}^{2n} \omega_i \boldsymbol{\gamma}_{i,k/k-1} = \sum_{i=0}^{2n} \omega_i h(\boldsymbol{\chi}'_{i,k/k-1}), \tag{10}$$

and its corresponding covariance matrix (innovation covariance matrix) is described as

$$\boldsymbol{P}_{\hat{\boldsymbol{z}}_{k/k-1}} = \sum_{i=0}^{2n} \omega_i \left(\boldsymbol{\gamma}_{i,k/k-1} - \hat{\boldsymbol{z}}_{k/k-1}\right)\left(\boldsymbol{\gamma}_{i,k/k-1} - \hat{\boldsymbol{z}}_{k/k-1}\right)^{\mathrm{T}} + \boldsymbol{R}_k. \tag{11}$$

The covariance between the predicted state and measurement is given by

$$\boldsymbol{P}_{\hat{\boldsymbol{x}}_{k/k-1}\hat{\boldsymbol{z}}_{k/k-1}} = \sum_{i=0}^{2n} \omega_i \left(\boldsymbol{\chi}_{i,k/k-1} - \hat{\boldsymbol{x}}_{k/k-1}\right) \times \left(\boldsymbol{\gamma}_{i,k/k-1} - \hat{\boldsymbol{z}}_{k/k-1}\right)^{\mathrm{T}}. \tag{12}$$

The Kalman gain can be computed as

$$\boldsymbol{K}_k = \boldsymbol{P}_{\hat{\boldsymbol{x}}_{k/k-1}\hat{\boldsymbol{z}}_{k/k-1}} \boldsymbol{P}^{-1}_{\hat{\boldsymbol{z}}_{k/k-1}}. \tag{13}$$

Based on the above process, the state estimate $\hat{\boldsymbol{x}}_k$ and associated error covariance matrix $\boldsymbol{P}_k$ are updated as

$$\hat{\boldsymbol{x}}_k = \hat{\boldsymbol{x}}_{k/k-1} + \boldsymbol{K}_k(\boldsymbol{z}_k - \hat{\boldsymbol{z}}_{k/k-1}), \tag{14}$$

$$\boldsymbol{P}_k = \boldsymbol{P}_{k/k-1} - \boldsymbol{K}_k \boldsymbol{P}_{\hat{\boldsymbol{z}}_{k/k-1}} \boldsymbol{K}_k^{\mathrm{T}}. \tag{15}$$

**Step 5:** Repeat Steps 2 to 4 for the next sample until all samples are processed.

It is obvious that if the system model (1) involves uncertainty, the predicted state $\hat{\boldsymbol{x}}_{k/k-1}$ and predicted measurement $\hat{\boldsymbol{z}}_{k/k-1}$ obtained by (6) and (10) will become inaccurate. This will further make the Kalman gain $\boldsymbol{K}_k$ biased, thus deteriorating the state estimate obtained from (14). Therefore, without accurate system model, the filtering solution of the classical UKF will be deteriorated or even divergent.

## 4. IMM ESTIMATION-BASED ADAPTIVE ROBUST UKF

### 4.1. Adaptive fading UKF and robust UKF

Assume uncertainty is involved in the process model of nonlinear system (1). The core idea of the AFUKF is to incorporate a time-varying adaptive fading factor into the predicted state covariance matrix which can refrain the influence of prior knowledge on the current state estimate [15]. Thus, the predicted state covariance matrix in the AFUKF is formulated as

$$\boldsymbol{P}^*_{k/k-1} = \lambda_k \left\{ \sum_{i=0}^{2n} \omega_i (\boldsymbol{\chi}_{i,k/k-1} - \hat{\boldsymbol{x}}_{k/k-1})(\boldsymbol{\chi}_{i,k/k-1} - \hat{\boldsymbol{x}}_{k/k-1})^{\mathrm{T}} + \boldsymbol{Q}_k \right\}, \tag{16}$$

where $\lambda_k$ is the adaptive fading factor.

On the contrary, when uncertainty is involved in the measurement model of nonlinear system (1), the basic idea of the RUKF is to embed a time-varying robust factor in the innovation covariance matrix to inhibit the disturbance of abnormal measurement on current state estimate [29]. The innovation covariance matrix in the RUKF is described as

$$\begin{aligned}&\boldsymbol{P}'_{\hat{\boldsymbol{z}}_{k/k-1}}\\&=s_k\left\{\sum_{i=0}^{2n}\omega_i\left(\boldsymbol{\gamma}_{i,k/k-1}-\hat{\boldsymbol{z}}_{k/k-1}\right)\left(\boldsymbol{\gamma}_{i,k/k-1}-\hat{\boldsymbol{z}}_{k/k-1}\right)^{\mathrm{T}}\right.\\&\left.+\boldsymbol{R}_k\right\},\end{aligned}\tag{17}$$

where $s_k$ is the robust factor.

Define the innovation vector as

$$\tilde{\boldsymbol{z}}_k=z_k-\hat{\boldsymbol{z}}_{k/k-1}.\tag{18}$$

As the classical UKF works under the optimal operational conditions, i.e., the nonlinear system described by (1) does not exist uncertainty, the following relationship can be fulfilled [30, 31]

$$\mathrm{E}\left[\tilde{\boldsymbol{z}}_k^{\mathrm{T}}\cdot\tilde{\boldsymbol{z}}_{k+j}\right]=0,\quad j=1,2,\cdots.\tag{19}$$

Equation (19) is called the principle of innovation orthogonality, which means that the innovation sequence has to be orthogonal to each other. This principle can guarantee that all the useful information in the innovation sequence can be extracted. The aforementioned adaptive fading factor and robust factor can be determined by compelling the relationship (19) to be held.

### 4.1.1 Determination of adaptive fading factor

Define the estimation error and prediction error as

$$\tilde{\boldsymbol{x}}_k=\boldsymbol{x}_k-\hat{\boldsymbol{x}}_k,\tag{20}$$

$$\tilde{\boldsymbol{x}}_{k/k-1}=\boldsymbol{x}_k-\hat{\boldsymbol{x}}_{k/k-1}.\tag{21}$$

Substituting (1) and (6) into (21) and expanding $f(\cdot)$ by a Taylor series about $\hat{\boldsymbol{x}}_{k-1}$, the prediction error is rewritten as

$$\tilde{\boldsymbol{x}}_{k/k-1}=\boldsymbol{F}_k\tilde{\boldsymbol{x}}_{k-1}+\Delta(\tilde{\boldsymbol{x}}_{k-1})+\boldsymbol{w}_k,\tag{22}$$

where $\boldsymbol{F}_k=\left.\frac{\partial f(\boldsymbol{x})}{\partial\boldsymbol{x}}\right|_{\boldsymbol{x}=\hat{\boldsymbol{x}}_{k-1}}$ and $\Delta(\tilde{\boldsymbol{x}}_{k-1})$ denotes the second and higher-order moments in the Taylor series.

For the purpose of simplifying the error expression, an unknown time-varying diagonal matrix $\boldsymbol{\beta}_k=diag(\boldsymbol{\beta}_{1,k},\boldsymbol{\beta}_{2,k},\cdots,\boldsymbol{\beta}_{n,k})$ is introduced to model the errors due to the first-order linearization [1, 9]. Thus, (22) becomes

$$\tilde{\boldsymbol{x}}_{k/k-1}=\boldsymbol{\beta}_k\boldsymbol{F}_k\tilde{\boldsymbol{x}}_{k-1}+\boldsymbol{w}_k.\tag{23}$$

Similar to the derivation process of $\tilde{\boldsymbol{x}}_{k/k-1}$, the innovation vector can be formulated by

$$\tilde{\boldsymbol{z}}_k=\boldsymbol{\alpha}_k\boldsymbol{H}_k\tilde{\boldsymbol{x}}_{k/k-1}+v_k,\tag{24}$$

where $\boldsymbol{H}_k=\left.\frac{\partial h(\boldsymbol{x})}{\partial\boldsymbol{x}}\right|_{\boldsymbol{x}=\hat{\boldsymbol{x}}_{k/k-1}}$ and $\boldsymbol{\alpha}_k=diag(\boldsymbol{\alpha}_{1,k},\boldsymbol{\alpha}_{2,k},\cdots,\boldsymbol{\alpha}_{m,k})$ is an unknown time-varying diagonal matrix.

From (24), we can obtain

$$\begin{aligned}\boldsymbol{P}_{\hat{\boldsymbol{z}}_{k/k-1}}&=\mathrm{E}\left[\left(\boldsymbol{z}_k-\hat{\boldsymbol{z}}_{k/k-1}\right)\left(\boldsymbol{z}_k-\hat{\boldsymbol{z}}_{k/k-1}\right)^{\mathrm{T}}\right]\\&=\boldsymbol{\alpha}_k\boldsymbol{H}_k\boldsymbol{P}_{k/k-1}\boldsymbol{H}_k^T\boldsymbol{\alpha}_k+R_k,\end{aligned}\tag{25}$$

$$\begin{aligned}\boldsymbol{P}_{\hat{\boldsymbol{x}}_{k/k-1}\hat{\boldsymbol{z}}_{k/k-1}}&=\mathrm{E}\left[\left(\boldsymbol{x}_k-\hat{\boldsymbol{x}}_{k/k-1}\right)\left(\boldsymbol{z}_k-\hat{\boldsymbol{z}}_{k/k-1}\right)^{\mathrm{T}}\right]\\&=\boldsymbol{P}_{k/k-1}\boldsymbol{H}_k^{\mathrm{T}}\boldsymbol{\alpha}_k.\end{aligned}\tag{26}$$

Denoting $\boldsymbol{Y}_{j,k}=\mathrm{E}\left[\tilde{\boldsymbol{z}}_{k+j}\tilde{\boldsymbol{z}}_k^{\mathrm{T}}\right]$, it can be achieved from (23) and (24)

$$\begin{aligned}\boldsymbol{Y}_{j,k}=&\mathrm{E}\left\{\left[\boldsymbol{\alpha}_{k+j}\boldsymbol{H}_{k+j}\left(\boldsymbol{\beta}_{k+j}\boldsymbol{F}_{k+j}\tilde{\boldsymbol{x}}_{k+j-1}+\boldsymbol{w}_{k+j}\right)+\boldsymbol{v}_{k+j}\right]\right.\\&\left.\times\left[\boldsymbol{\alpha}_k\boldsymbol{H}_k\left(\boldsymbol{\beta}_k\boldsymbol{F}_k\tilde{\boldsymbol{x}}_{k-1}+\boldsymbol{w}_k\right)+\boldsymbol{v}_k\right]^{\mathrm{T}}\right\}\\=&\boldsymbol{\alpha}_{k+j}\boldsymbol{H}_{k+j}\boldsymbol{\beta}_{k+j}\boldsymbol{F}_{k+j}\cdot\left(\prod_{i=k+1}^{k+j-1}\left(\boldsymbol{I}-\boldsymbol{K}_i\boldsymbol{\alpha}_i\boldsymbol{H}_i\right)\boldsymbol{\beta}_i\boldsymbol{F}_i\right)\\&\times\left(\hat{\boldsymbol{P}}_{\hat{\boldsymbol{x}}_{k/k-1}\hat{\boldsymbol{z}}_{k/k-1}}-\boldsymbol{K}_k\boldsymbol{Y}_{0,k}\right),\end{aligned}\tag{27}$$

where $\boldsymbol{Y}_{0,k}$ is the actual innovation covariance and can be calculated as [31]

$$\boldsymbol{Y}_{0,k}=\begin{cases}\tilde{\boldsymbol{z}}_1\tilde{\boldsymbol{z}}_1^{\mathrm{T}}, & k=1,\\ \dfrac{\rho\cdot\boldsymbol{Y}_{0,k-1}+\tilde{\boldsymbol{z}}_k\tilde{\boldsymbol{z}}_k^{\mathrm{T}}}{1+\rho}, & k>1,\end{cases}\tag{28}$$

in which $0<\rho\leq 1$ is a forgetting factor and is generally chosen as $\rho=0.95$.

Letting $\boldsymbol{Y}_{j,k}=0$, we have

$$\boldsymbol{P}_{\hat{\boldsymbol{x}}_{k/k-1}\hat{\boldsymbol{z}}_{k/k-1}}-\boldsymbol{K}_k\boldsymbol{Y}_{0,k}=\boldsymbol{0}.\tag{29}$$

Substituting the modified prediction covariance matrix (16) into (25), the innovation covariance matrix is redefined as

$$\begin{aligned}\boldsymbol{P}^*_{\hat{\boldsymbol{z}}_{k/k-1}}=&\boldsymbol{\alpha}_k\boldsymbol{H}_k\boldsymbol{P}^*_{k/k-1}\boldsymbol{H}_k^{\mathrm{T}}\alpha_k+\boldsymbol{R}_k\\=&\lambda_k\boldsymbol{\alpha}_k\boldsymbol{H}_k\boldsymbol{P}_{k/k-1}\boldsymbol{H}_k^{\mathrm{T}}\boldsymbol{\alpha}_k+\boldsymbol{R}_k.\end{aligned}\tag{30}$$

Similarly, the covariance between the predicted state and measurement can be modified as

$$\boldsymbol{P}^*_{\hat{\boldsymbol{x}}_{k/k-1}\hat{\boldsymbol{z}}_{k/k-1}}=\boldsymbol{P}^*_{k/k-1}\boldsymbol{H}_k^{\mathrm{T}}\boldsymbol{\alpha}_k=\lambda_k\boldsymbol{P}_{k/k-1}\boldsymbol{H}_k^{\mathrm{T}}\boldsymbol{\alpha}_k.\tag{31}$$

Substituting (30) and (31) into (29) and further making it hold, it is verified that

$$\boldsymbol{Y}_{0,k}-\boldsymbol{R}_k=\lambda_k\boldsymbol{\alpha}_k\boldsymbol{H}_k\boldsymbol{P}_{k/k-1}\boldsymbol{H}_k^{\mathrm{T}}\boldsymbol{\alpha}_k=\lambda_k\left(\boldsymbol{P}_{\hat{\boldsymbol{z}}_{k/k-1}}-\boldsymbol{R}_k\right).\tag{32}$$

Embedding (11) into (32), we can obtain

$$\lambda_k \sum_{i=0}^{2n} \omega_i \left(\boldsymbol{\gamma}_{i,k/k-1} - \hat{\boldsymbol{z}}_{k/k-1}\right)\left(\boldsymbol{\gamma}_{i,k/k-1} - \hat{\boldsymbol{z}}_{k/k-1}\right)^{\mathrm{T}} = \boldsymbol{Y}_{0,k} - \mathbf{R}_k. \tag{33}$$

Taking the trace of both sides of (33), the adaptive fading factor can be determined as

$$\lambda_k = \frac{tr\left(\boldsymbol{Y}_{0,k} - \boldsymbol{R}_k\right)}{tr\left(\sum_{i=0}^{2n} \omega_i \left(\boldsymbol{\gamma}_{i,k/k-1} - \hat{\boldsymbol{z}}_{k/k-1}\right)\left(\boldsymbol{\gamma}_{i,k/k-1} - \hat{\boldsymbol{z}}_{k/k-1}\right)^{\mathrm{T}}\right)}. \tag{34}$$

It should be noted that the $\lambda_k$ in (34) may be less than 1. To avoid this situation, the adaptive fading factor can be further chosen as

$$\lambda_k = \max\left\{1, \frac{tr\left(\boldsymbol{Y}_{0,k} - \boldsymbol{R}_k\right)}{tr\left(\sum_{i=0}^{2n} \omega_i \left(\boldsymbol{\gamma}_{i,k/k-1} - \hat{\boldsymbol{z}}_{k/k-1}\right)\left(\boldsymbol{\gamma}_{i,k/k-1} - \hat{\boldsymbol{z}}_{k/k-1}\right)^{\mathrm{T}}\right)}\right\}. \tag{35}$$

### 4.1.2 Determination of robust factor

The robust factor $s_k$ can also be determined in a similar way as the derivation process of $\lambda_k$. Substituting the modified innovation covariance matrix (17) into (29) and further making it hold, it is verified that

$$\boldsymbol{P}'_{\hat{z}_{k/k-1}} = \boldsymbol{Y}_{0,k}, \tag{36}$$

that is,

$$s_k \left\{\sum_{i=0}^{2n} \omega_i \left(\boldsymbol{\gamma}_{i,k/k-1} - \hat{\boldsymbol{z}}_{k/k-1}\right)\left(\boldsymbol{\gamma}_{i,k/k-1} - \hat{\boldsymbol{z}}_{k/k-1}\right)^{\mathrm{T}} + \boldsymbol{R}_k\right\} = \boldsymbol{Y}_{0,k}. \tag{37}$$

By taking the trace of both sides of (37), we obtain the robust factor

$$s_k = \frac{tr\left(\boldsymbol{Y}_{0,k}\right)}{tr\left(\sum_{i=0}^{2n} \omega_i \left(\boldsymbol{\gamma}_{i,k/k-1} - \hat{\boldsymbol{z}}_{k/k-1}\right)\left(\boldsymbol{\gamma}_{i,k/k-1} - \hat{\boldsymbol{z}}_{k/k-1}\right)^{\mathrm{T}} + \boldsymbol{R}_k\right)}. \tag{38}$$

To avoid $s_k$ less than 1, the robust factor is also further chosen as

$$s_k = \max\left\{1, \frac{tr\left(\boldsymbol{Y}_{0,k}\right)}{tr\left(\sum_{i=0}^{2n} \omega_i \left(\boldsymbol{\gamma}_{i,k/k-1} - \hat{\boldsymbol{z}}_{k/k-1}\right)\left(\boldsymbol{\gamma}_{i,k/k-1} - \hat{\boldsymbol{z}}_{k/k-1}\right)^{\mathrm{T}} + \boldsymbol{R}_k\right)}\right\}. \tag{39}$$

## 4.2. Multi-filter fusion by IMM estimation

It can be seen from the above analysis that the AFUKF only handles process model uncertainty while the RUKF only handles measurement model uncertainty. Therefore, the above two filters have complementary features with each other. This section will develop an IMM estimation method to fuse the AFUKF and RUKF to combine their merits and discard their limitations. As shown in Fig. 1, this method uses a multi-filter fusion process, where the AFUKF and RUKF are run as two sub-filters in parallel, each matching a particular system mode. One sub-filter is the AFUKF for the case in presence of process model uncertainty only, while the other is the RUKF for the case in presence of measurement model uncertainty only. The probability of transition between both sub-filters is governed by a Markov chain. The overall state estimate is obtained by combination of all the state estimates from each sub-filter.

### 4.2.1 Initialization

For the initialization of the multi-filter fusion, the following Markov transition matrix and the initial mode probability are defined as

$$\boldsymbol{M} = \begin{bmatrix} m_{11} & m_{12} \\ m_{21} & m_{22} \end{bmatrix}, \quad \boldsymbol{\mu}_0 = \begin{bmatrix} \boldsymbol{\mu}_{1,0} \\ \boldsymbol{\mu}_{2,0} \end{bmatrix}, \tag{40}$$

where $m_{ij}$ is the Markov transition probability from sub-filter $i$ to sub-filter $j$; and the mode probability describes

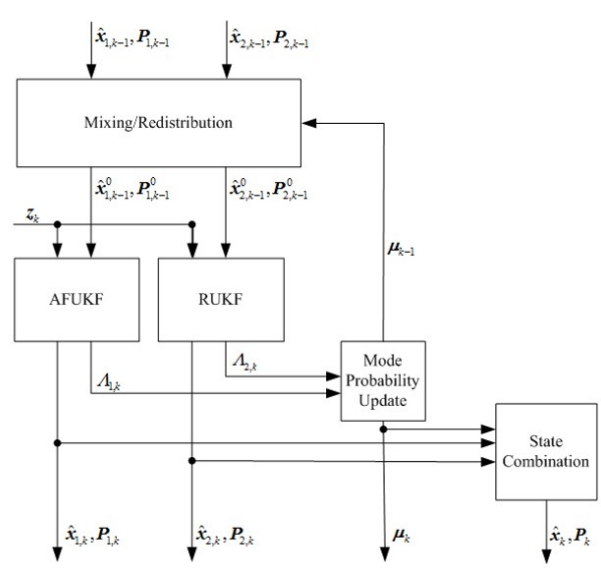


Fig. 1. The architecture of the IMM estimation.

the reliability of each sub-filter as probability at current time. Thus, the summation of the elements for each column is 1.

Then, the normalization factor is set as

$$\boldsymbol{c}_0 = \boldsymbol{M}^{\mathrm{T}}\boldsymbol{\mu}_0 = \begin{bmatrix} c_{1,0} & c_{2,0} \end{bmatrix}^T. \tag{41}$$

### 4.2.2 Mode probability update

To fuse the two sub-filters, the mode probability should be firstly updated with the innovation vectors and the innovation covariance matrices of the two sub-filters

$$\mu_{j,k} = \frac{\Lambda_{j,k} c_{j,k-1}}{\sum_{j=1}^{2} \Lambda_{j,k} c_{j,k-1}} \quad (j = 1,2), \tag{42}$$

where $\mu_{j,k}$ is the mode probability of sub-filter $j$, and $\Lambda_{j,k}$ is the likelihood function of sub-filter $j$ at time $k$ which is computed as

$$\Lambda_{j,k} = \frac{1}{\sqrt{(2\pi)^m \left|\boldsymbol{P}^j_{\hat{\boldsymbol{z}}_{k/k-1}}\right|}} \exp\left\{-\frac{1}{2}\tilde{\boldsymbol{z}}^{\mathrm{T}}_{j,k}\left(\boldsymbol{P}^j_{\hat{\boldsymbol{z}}_{k/k-1}}\right)^{-1}\tilde{\boldsymbol{z}}_{j,k}\right\}, \tag{43}$$

where $\tilde{\boldsymbol{z}}_{j,k}$ is the innovation vector of sub-filter $j$ at time $k$, $\boldsymbol{P}^j_{\hat{\boldsymbol{z}}_{k/k-1}}$ is the corresponding innovation covariance matrix, and $m$ is the dimension of measurement vector $\boldsymbol{z}_k$.

The innovation covariance matrices of the AFUKF and RUKF are respectively calculated as

$$\boldsymbol{P}^1_{\hat{\boldsymbol{z}}_{k/k-1}} = \sum_{i=0}^{2n} \omega_i \left(\boldsymbol{\gamma}^1_{i,k/k-1} - \hat{\boldsymbol{z}}^1_{k/k-1}\right)\left(\boldsymbol{\gamma}^1_{i,k/k-1} - \hat{\boldsymbol{z}}^1_{k/k-1}\right)^{\mathrm{T}} + \boldsymbol{R}_k, \tag{44}$$

$$\boldsymbol{P}^2_{\hat{\boldsymbol{z}}_{k/k-1}} = s_k \left\{\sum_{i=0}^{2n} \omega_i \left(\boldsymbol{\gamma}^2_{i,k/k-1} - \hat{\boldsymbol{z}}^2_{k/k-1}\right)\left(\boldsymbol{\gamma}^2_{i,k/k-1} - \hat{\boldsymbol{z}}^2_{k/k-1}\right)^{\mathrm{T}} + \boldsymbol{R}_k\right\}, \tag{45}$$

where $\boldsymbol{\gamma}^j_{k/k-1}$ is the transformed sigma points through the measurement function in sub-filter $j$, and $\hat{\boldsymbol{z}}^j_{k/k-1}$ is the predicted measurement of sub-filter $j$.

In (42) and (43), the likelihood function $\Lambda_{j,k}$ characterizes the relative performance of one sub-filter with respect to the other. It can be seen from (43) that the closer to zero the innovation vector $\tilde{\boldsymbol{z}}_{j,k}$ is, which means the sub-filter matches the actual system more closely, the large $\Lambda_{j,k}$ will be, leading to the larger mode probability for the sub-filter. If process model uncertainty is more significant than measurement model uncertainty, the AFUKF will have the larger $\Lambda_{j,k}$ than the RUKF, leading to the larger mode probability for the AFUKF. On the contrary, if measurement model uncertainty is more significant than process model uncertainty, the RUKF will have the larger mode probability than the AFUKF. Therefore, the IMM estimation always follows a sub-filter, which is the one that outperforms the other.

### 4.2.3 Mixing/redistribution

The states $\hat{\boldsymbol{x}}_{j,k}$ and the corresponding error covariance matrices $\boldsymbol{P}_{j,k}$ of the two sub-filters are redistributed as

$$\hat{\boldsymbol{x}}^0_{i,k} = \sum_{j=1}^{2} \hat{\boldsymbol{x}}_{j,k} g_{ij,k} \quad (i = 1,2), \tag{46}$$

$$\boldsymbol{P}^0_{i,k} = \sum_{j=1}^{2} \left\{\boldsymbol{P}_{j,k} + \left[\hat{\boldsymbol{x}}_{j,k} - \hat{\boldsymbol{x}}^0_{i,k}\right]\left[\hat{\boldsymbol{x}}_{j,k} - \hat{\boldsymbol{x}}^0_{i,k}\right]^{\mathrm{T}}\right\} g_{ij,k} \quad (i = 1,2), \tag{47}$$

where $g_{ij,k}$ is the mixing probability, which is calculated as

$$g_{ij,k} = \frac{m_{ij}\mu_{j,k}}{c_{i,k}}, \quad g_{1j,k} + g_{2j,k} = 1, \tag{48}$$

where $\mu_{j,k}$ is the updated mode probability, $m_{ij}$ is the preset Markov transition probability, and $c_{i,k} = \sum_{j=1}^{2} m_{ij}\mu_{j,k}$, $(i = 1, 2)$ is the normalization factor and is reused in the mode probability update at the next time step.

Subsequently, the redistributed states and error covariance matrices are sent to each sub-filter as the initial values for the calculation at the next time step.

### 4.2.4 State combination

The overall state estimation and error covariance matrix can be obtained via the states and error covariance matrices of the two sub-filters and the mode probability as

$$\hat{\boldsymbol{x}}_k = \sum_{j=1}^{2} \hat{\boldsymbol{x}}_{j,k}\mu_{j,k}, \tag{49}$$

$$\boldsymbol{P}_k = \sum_{j=1}^{2} \left\{\boldsymbol{P}_{j,k} + \left[\hat{\boldsymbol{x}}_{j,k} - \hat{\boldsymbol{x}}_k\right]\left[\hat{\boldsymbol{x}}_{j,k} - \hat{\boldsymbol{x}}_k\right]^{\mathrm{T}}\right\}\mu_{j,k}. \tag{50}$$

## 4.3. IMM estimation-based adaptive robust UKF

It can also be seen from Fig. 1 that the AFUKF and RUKF are performed independently, and subsequently their filtering results are fused using the IMM estimation to obtain the overall state estimation. The procedure of the proposed IMM-ARUKF involves the following main steps:

**Step 1:** *Initialization.* This step is to initialize the two sub-filters and multi-filter fusion process.

(i) The AFUKF and RUKF can be initialized as

$$\begin{cases} \hat{\boldsymbol{x}}_{j,0} = \mathrm{E}[\boldsymbol{x}_{j,0}] \\ \boldsymbol{P}_{j,0} = \mathrm{E}\left[(\boldsymbol{x}_{j,0} - \hat{\boldsymbol{x}}_{j,0})(\boldsymbol{x}_{j,0} - \hat{\boldsymbol{x}}_{j,0})^{\mathrm{T}}\right] \end{cases} (j = 1,2). \tag{51}$$

(ii) The initialization of the multi-filter fusion process is conducted by presetting the Markov transition matrix and the initial mode probability as (40).

**Step 2:** *Parallel Filter.* This step performs the AFUKF and RUKF in a parallel structure to obtain the associated state estimation $\hat{\boldsymbol{x}}_{j,k}$ and the error covariance matrix $\boldsymbol{P}_{j,k}$.

(i) The AFUKF is implemented by replacing the predicted state covariance matrix $\boldsymbol{P}_{k/k-1}$ of the classical UKF with the modified type $\boldsymbol{P}^{*}_{k/k-1}$ as described by (16). The other procedures are same with the classical UKF.

(ii) Different with the AFUKF, the RUKF is performed by modifying the innovation covariance matrix $\boldsymbol{P}_{\hat{z}_{k/k-1}}$ of the classical UKF as $\boldsymbol{P}'_{\hat{z}_{k/k-1}}$ given by (17).

**Step 3:** *Multi-Filter Fusion.* Based on the IMM estimation method discussed in Section 4.2, by (40)-(50), the overall system state estimation and associated error covariance matrix can be described as

$$\hat{\boldsymbol{x}}_k = \sum_{j=1}^{2} \hat{\boldsymbol{x}}_{j,k} \mu_{j,k}, \tag{52}$$

$$\boldsymbol{P}_k = \sum_{j=1}^{2} \left\{ \boldsymbol{P}_{j,k} + [\hat{\boldsymbol{x}}_{j,k} - \hat{\boldsymbol{x}}_k] [\hat{\boldsymbol{x}}_{j,k} - \hat{\boldsymbol{x}}_k]^{\mathrm{T}} \right\} \mu_{j,k}. \tag{53}$$

**Step 4:** Repeat Steps 2 to 3 for the next sample until all samples are processed.

## 5. PERFORMANCE EVALUATION AND DISCUSSION

Numerical simulations and practical experiments have been conducted to comprehensively evaluate the performance of the proposed IMM-ARUKF. Comparison analysis of the proposed IMM-ARUKF with the classical UKF, AFUKF and RUKF is also discussed in this section.

### 5.1. Numerical simulations and analysis

The univariate nonstationary growth model [32, 33] is used to conduct numerical simulations to evaluate the performance of the proposed IMM-ARUKF. The corresponding discrete-time dynamic system model is described as

$$x_k = 0.5x_{k-1} + 25x_{k-1}/(1+x_{k-1}^2) + 8\cos[1.2(k-1)] + w_k, \tag{54}$$

$$z_k = x_k^2/20 + v_k, \tag{55}$$

where $w_k$ and $v_k$ are the uncorrelated zero-mean Gaussian white noises with covariances $Q_k = 10$ and $R_k = 3$.

The initial state and its error covariance of the dynamic system were chosen as

$$\hat{x}_0 = 0.1, \quad P_0 = 1. \tag{56}$$

The initial true state for generating the reference value at each time step was set as

$$x_0 = 0.1. \tag{57}$$

The initial Markov transition matrix and initial mode probability for the proposed IMM-ARUKF were chosen as

$$\boldsymbol{M} = \begin{bmatrix} 0.5 & 0.5 \\ 0.5 & 0.5 \end{bmatrix}, \quad \boldsymbol{\mu}_0 = \begin{bmatrix} 0.5 \\ 0.5 \end{bmatrix}. \tag{58}$$

Trials were conducted under various types of system model uncertainty including model parameter mismatch, system noise statistic error and stochastic drifts. The simulation time step for each type of system model uncertainty is 500. The estimation error of the proposed IMM-ARUKF was evaluated by 200 times of Monte Carlo simulations and compared with the classical UKF, AFUKF and RUKF in terms of the root mean squared error (RMSE) that is defined as

$$RMSE = \left( \frac{1}{N} \sum_{i=1}^{N} [(\hat{x}_k - x_k)_i]^2 \right)^{\frac{1}{2}}, \quad N = 200. \tag{59}$$

**Case 1: Model parameter mismatch**

In order to evaluate the performance of the proposed IMM-ARUKF in terms of model parameter mismatch, two different modifications are applied to the process model and measurement model, respectively. During the time interval (100, 200) the process model was changed to

$$x_k = x_{k-1} + 30x_{k-1}/(1+x_{k-1}^2) + 10\cos[1.2(k-1)] + w_k. \tag{60}$$

During the time interval (300, 400) the measurement model was modified as

$$z_k = x_k^2/5 + v_k. \tag{61}$$

It is obvious that (60) and (61) involves model uncertainty due to the parameter mismatch.

Fig. 2 illustrates the RMSEs of state $x_k$ obtained by the classical UKF, AFUKF, RUKF and proposed IMM-ARUKF, respectively. Table 1 lists the mean RMSEs of

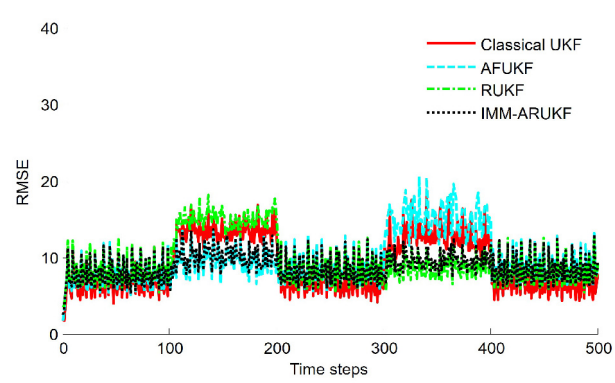


Fig. 2. RMSEs of state $x_k$ by the classical UKF, AFUKF, RUKF and proposed IMM-ARUKF for Case 1.

state $x_k$ by the classical UKF, AFUKF, RUKF and proposed IMM-ARUKF for the case of model parameter mismatch during the time intervals (100, 200) and (300, 400). It can be seen from Fig. 2 that, during the time interval (100, 200), the classical UKF is significantly disturbed by the mismatched process model parameters, resulting in a large estimation error with the mean RMSE of 13.3173. The AFUKF can effectively resist the influence due to the process model parameter mismatch on the filtering solution and improves the estimation accuracy of the classical UKF. The mean RMSE of state $x_k$ obtained by the AFUKF is 9.4072. However, the mean RMSE of state $x_k$ achieved by the RUKF is 14.7850, which is even worse than that of the classical UKF. This is because the RUKF does not have the capability to handle process model uncertainty, thus deteriorating the filtering solution. Since the proposed IMM-ARUKF always follows the sub-filter that outperforms the other (i.e., the AFUKF in this case), the resultant filtering solution is close to that of the AFUKF. The mean RMSE of the IMM-ARUKF is 10.0139, which is very close to that of the AFUKF and is also much smaller than those of the classical UKF and RUKF.

For the time interval (300, 400) involving the measurement model parameter mismatch, the classical UKF is also disturbed by the mismatched measurement model parameters, leading to the mean RMSE of 12.4923. The AFUKF accuracy is worse than that of the classical UKF, since it does not have the capability to handle measurement model uncertainty, while the RUKF can improve the performance of the classical UKF by introducing the robust factor to weaken the disturbance of measurement model uncertainty. The mean RMSEs obtained by the AFUKF and RUKF are 15.0753 and 8.7049, respectively. As the RUKF has a better filtering performance than the AFUKF, the IMM-ARUKF follows the RUKF, leading to the mean RMSE of 9.4604, which is very close to that of the RUKF.

It should be noted that since both the AFUKF and RUKF are essentially a suboptimal method, their estimation errors are slightly larger than that of the classical UKF in the time intervals (0, 100), (200, 300) and (400, 500) without system model uncertainty. Consequently, the proposed IMM-ARUKF is also a suboptimal filter and its estimation error is also slightly larger than that of the classical UKF in the time intervals without system model uncertainty. However, in practice, due to the effect of the dynamic environment, uncertainty is always existed in both process and measurement models, as shown in the experimental case in Section 5.2.

**Case 2: System noise statistic error**

The similar strategy used in the case of model parameter mismatch is also used to evaluate the performance of the proposed IMM-ARUKF in terms of system noise statistics error. Two modifications were applied to the two time intervals (100, 200) and (300, 400), leading to a large bias between the initial and real values for both process noise covariance $Q_k$ and measurement noise covariance $R_k$. The process noise covariance was enlarged to 10 times of its initial value in the time interval (100, 200) and the measurement noise covariance was enlarged to 100 times of its initial value in the time interval (300, 400), i.e.,

$$Q_k = \begin{cases} 10, & k \le 100, \\ 100, & 100 < k \le 200, \\ 10, & 200 < k \le 500, \end{cases}$$
$$R_k = \begin{cases} 3, & k \le 300, \\ 300, & 300 < k \le 400, \\ 3, & 400 < k \le 500. \end{cases} \tag{62}$$

The RMSEs of state $x_k$ obtained by the classical UKF, AFUKF, RUKF and proposed IMM-ARUKF are shown in Fig. 3. Table 1 also shows the mean RMSEs of state $x_k$ by the classical UKF, AFUKF, RUKF and proposed IMM-ARUKF for the case of system noise statistic error during the time intervals (100, 200) and (300, 400). It can be seen that during the time interval (100, 200) with process noise statistics error, the estimation accuracy of the classical UKF and RUKF is deteriorated significantly, leading to the mean RMSEs of 12.2395 and 14.3971, respectively. The AFUKF decreases the estimation error to the mean RMSE of 9.5048 by introducing the adaptive fading factor to inhibit the disturbance of process model uncertainty. As the proposed IMM-ARUKF follows the sub-filter that outperforms the other (i.e., the AFUKF in this case ), it also has a small estimation error with the mean RMSE of 10.2386 in the time interval (100, 200). The similar trend can also be found for the time interval (300, 400) with the measurement noise statistics error, where the mean RMSE of state $x_k$ is 13.1552 for the classical UKF, 14.5959 for the AFUKF, and 8.9610 for the RUKF. Because the proposed IMM-ARUKF follows the RUKF that outperforms the AFUKF in this time period, its mean RMSE is 9.8062, which is much smaller than those of the classical UKF and AFUKF.

**Case 3: Stochastic drifts**

Suppose that the system model involves the uncertainty of stochastic drifts. Similar to the above two cases, the following process model with stochastic drifts is adopted during the time interval (100, 200)

$$\begin{aligned} x_k =& 0.5x_{k-1} + 25x_{k-1}/(1+x_{k-1}^2) + 8\cos[1.2(k-1)] \\ &+ 25\mathrm{rand}(k) + w_k \end{aligned} \tag{63}$$

and the following measurement model with stochastic drifts is adopted during the time interval (300, 400)

$$z_k = x_k^2/20 + 50\mathrm{rand}(k) + v_k \tag{64}$$

where $\mathrm{rand}(k)$ is a pseudorandom number drawn from the standard uniform distribution at time step $k$. It should be

Table 1. Mean RMSEs of the state $x_k$ by the classical UKF, AFUKF, RUKF and proposed IMM-ARUKF during the time intervals (100, 200) and (300, 400) for the simulation case.

| | | Classical UKF | AFUKF | RUKF | IMM-ARUKF |
|---|---|---|---|---|---|
| Case 1 | (100, 200) | 13.3173 | 9.4072 | 14.7850 | 10.0139 |
| | (300, 400) | 12.4923 | 15.0753 | 8.7049 | 9.4604 |
| Case 2 | (100, 200) | 12.2395 | 9.5048 | 14.3971 | 10.2386 |
| | (300, 400) | 13.1552 | 14.5959 | 8.9610 | 9.8062 |
| Case 3 | (100, 200) | 19.1809 | 11.9642 | 20.9689 | 12.5451 |
| | (300, 400) | 14.7836 | 16.9041 | 9.0675 | 9.9430 |

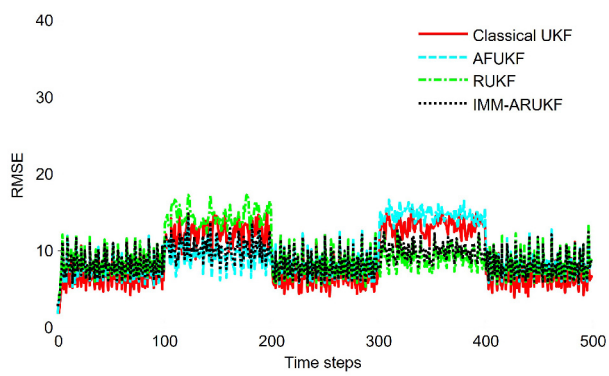


Fig. 3. RMSEs of the state $x_k$ by the classical UKF, AFUKF, RUKF and proposed IMM-ARUKF for Case 2.

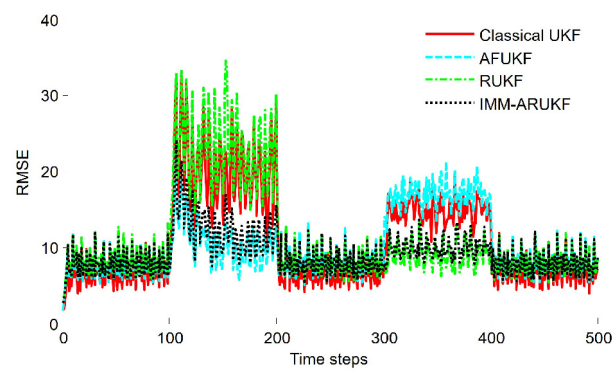


Fig. 4. RMSEs of the state $x_k$ by the classical UKF, AFUKF, RUKF and proposed IMM-ARUKF for Case 3.

noted that the covariance of the system noise in this case is identical to those described by (54) and (55).

The RMSEs of state $x_k$ achieved by the classical UKF, AFUKF, RUKF and proposed IMM-ARUKF are depicted in Fig. 4 and their mean RMSEs during the time intervals (100, 200) and (300, 400) are also listed in Table 1. Fig. 4 shows the similar phenomenon as the cases of model parameter mismatch and system noise statistic error. As shown in Fig. 4, the classical UKF has large estimation errors with the mean RMSEs of 19.1809 and 14.7836 during the time intervals (100, 200) and (300, 400). Comparing with the classical UKF, the AFUKF improves the filtering performance to the mean RMSE of 11.9642 for the time interval (100, 200), while it deteriorates the filtering performance to the mean RMSE of 20.9689 for the time interval (300, 400). On the contrary, compared to the classical UKF, the RUKF increases the estimation error to the mean RMSE of 16.9041 for the time interval (100, 200) and decreases the estimation error to the mean RMSE of 9.0675 for the time interval (300, 400). The proposed IMM-ARUKF follows the AFUKF that outperforms the RUKF during the time interval (100, 200) and follows the RUKF that outperforms the AFUKF during the time interval (300, 400), leading to the mean RMSEs of 12.5451 and 9.9430 in these two time intervals, respectively.

The above numerical simulation results and analysis demonstrate that the proposed IMM-ARUKF has a strong ability to inhibit the disturbances on the filtering solution due to system model uncertainties such as model parameter mismatch, system noise statistic error and stochastic drifts. It overcomes the limitation of the classical UKF in requiring accurately described system model. Further, it also inherits the merits and overcomes the demerits of the AFUKF and RUKF, leading to improved adaptability and robustness.

## 5.2. Experiments and analysis

For the performance evaluation of the proposed IMM-ARUKF, a practical experiment was also conducted for vehicle navigation. As shown in Fig. 5, the vehicle used an INS/GPS (Inertial Navigation System/Global Positioning System) integration system for navigation and positioning. This navigation system consists of a Guanxing NV-IMU300 inertial measurement unit and a JAVAD Lexon-GGD112T GPS receiver with the output of C/A GPS data at 1Hz. Moreover, another JAVAD Lexon-GGD112T GPS receiver, which was placed at a local reference station, was used along with the one mounted on the vehicle to provide the differential GPS (DGPS) data at 1Hz. The maximal distance between the vehicle and the local reference station was less than 60 km to achieve the position accuracy of less than 0.1 m from the DGPS via post difference processing. The DGPS data were used as the reference values for the comparison with the filtering results from the C/A

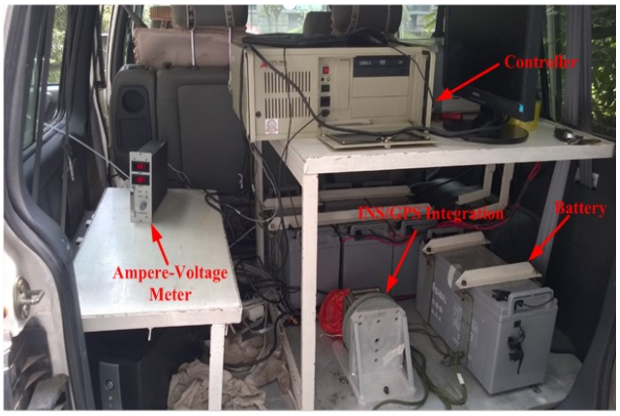


Fig. 5. Experimental setup for the vehicle navigation.

Fig. 6. Vehicle trajectory.

code measurements of the INS/GPS integration system.

The navigation frame for the INS/GPS integration is chosen as the E-N-U (East-North-Up) geography frame. The process model of the INS/GPS integration consists of the INS mechanical calibration equations and inertial sensor error equations. The system state vector $\boldsymbol{x}$ is defined as

$$\boldsymbol{x}(t) = [\psi, \theta, \gamma, v_E, v_N, v_U, L, \lambda, h, \varepsilon_x, \varepsilon_y, \varepsilon_z, \nabla_x, \nabla_y, \nabla_z]^{\mathrm{T}}, \tag{65}$$

where $\psi$, $\theta$ and $\gamma$ are the yaw, pitch and roll angels; $(v_E, v_N, v_U)$ is the velocity in the East, North and Up; $(L, \lambda, h)$ is the position in latitude, longitude, and altitude; $(\varepsilon_x, \varepsilon_y, \varepsilon_z)$ is the gyro constant drift; and $(\nabla_x, \nabla_y, \nabla_z)$ is the accelerometer constant bias.

The process model is described as

$$\dot{\boldsymbol{x}}(t) = f(\boldsymbol{x}(t)) + \boldsymbol{w}(t), \tag{66}$$

where $f(\cdot)$ and $\boldsymbol{w}(t)$ denote the nonlinear function describing the process model and the process noise, respectively [34].

The measurement model for the INS/GPS integration is established by use of the velocity and position output from the GPS receiver. The corresponding measurement vector $\boldsymbol{z}$ is chosen as

$$\boldsymbol{z} = [v_{EG}, v_{NG}, v_{UG}, L_G, \lambda_G, h_G]^{\mathrm{T}}. \tag{67}$$

The measurement equation is given by [34]

$$\boldsymbol{z}_k = \boldsymbol{H}_k \boldsymbol{x}_k + \boldsymbol{v}_k, \tag{68}$$

where $\boldsymbol{H}_k = [\boldsymbol{0}_{6\times3}, \boldsymbol{I}_{6\times6}, \boldsymbol{0}_{6\times6}]$, and $\boldsymbol{v}_k$ is the measurement noise vector.

The vehicle navigation test was carried out from the Northwestern Polytechnical University (NWPU) to Guodu, both in Xi'an, China. The vehicle trajectory is shown in Fig. 6. The start position of the vehicle was at North latitude 34.026°, East longitude 108.765°, and altitude 439 m. The initial velocities were 10 m/s, 10 m/s and 0 m/s in the East, North and Up. The gyro constant drift was 0.1∘/h, and its white noise was 0.05∘/h. The accelerometer zero bias was $10^{-3}$g, and its white noise was $10^{-4}$g. The GPS receiver's horizontal position error (RMS) was 5 m, the altitude error (RMS) 8 m, and the velocity error (RMS) 0.05 m/s. The vehicle's initial position error was (12 m, 12 m, 15 m), initial velocity error (0.3 m/s, 0.3 m/s, 0.3 m/s), and initial attitude error $(1.5', 1', 1')$. The test time was 2000 s and the filtering period was 1s. The initial Markov transition matrix and the initial mode probability for the proposed IMM-ARUKF were chosen as

$$\boldsymbol{M} = \begin{bmatrix} 0.4 & 0.6 \\ 0.6 & 0.4 \end{bmatrix}, \quad \boldsymbol{\mu}_0 = \begin{bmatrix} 0.4 \\ 0.6 \end{bmatrix}. \tag{69}$$

Figs. 7-8 illustrate the longitude and latitude errors of the vehicle achieved by the classical UKF, AFUKF, RUKF and proposed IMM-ARUKF, respectively. As the navigation system mounted on the vehicle is disturbed by the dynamic environment during the testing process, the INS/GPS integration involves various uncertainties in the process and measurement models. It can be observed from Figs. 7-8 that, the filtering accuracy of the classical UKF is significantly distributed by the uncertainties involved in the system model, leading to a large magnitude of oscillations in the error curve. During the time period (200 s, 2000 s), the position errors in longitude and latitude by the classical UKF are within (−23.4751 m, 22.1239 m) and (−24.5960 m, 22.0306 m), respectively. Comparing to the classical UKF, the AFUKF improves the filtering performance and the position errors in longitude and latitude are within (−15.3349 m, 13.1350 m) and (−17.1742 m, 16.4747 m). Similarly, the RUKF also improves the filtering performance of the classical UKF, leading to the position errors in longitude and latitude within (−14.4137

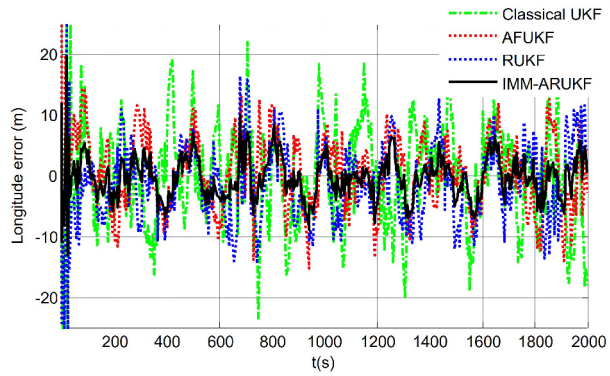


Fig. 7. The longitude errors obtained by the classical UKF, AFUKF, RUKF and proposed IMM-ARUKF for the vehicle navigation case.

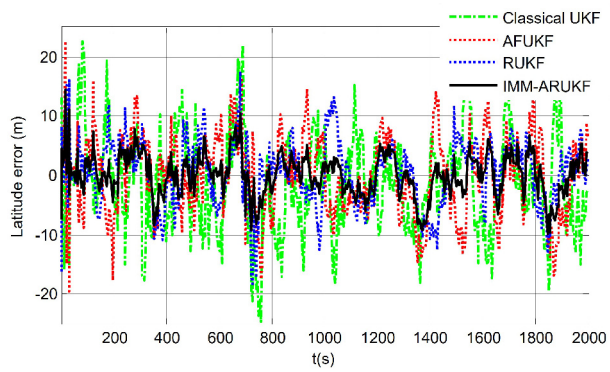


Fig. 8. The latitude errors obtained by the classical UKF, AFUKF, RUKF and proposed IMM-ARUKF for the vehicle navigation case.

m, 16.4688 m) and (−18.2539 m, 17.4727 m). However, obvious oscillations still remain in the error curves of the AFUKF and RUKF. This is because the AFUKF only considers process model uncertainty without the capability to handle measurement model uncertainty, while the RUKF only considers the measurement model uncertainty without the capability to control process model uncertainty. Compared with the above three methods, the position errors in longitude and latitude obtained by the proposed IMM-ARUKF are within (−8.9201 m, 9.9811 m) and (−9.9312 m, 10.5010 m), which are much smaller than those of the classical UKF, AFUKF and RUKF. The reason is that the proposed IMM-ARUKF can handle both process model uncertainty and measurement model uncertainty simultaneously by dynamically fusing the AFUKF and RUKF to compensate their individual errors and further follow one of them with better filtering solution. This indicates that the proposed IMM-ARUKF has stronger adaptability and robustness against uncertainties in both process and measurement models than the AFUKF and RUKF, resulting in a higher navigation accuracy than the classical UKF, AFUKF and RUKF.

Table 2. MAEs and STDs of the position errors by the classical UKF, AFUKF, RUKF and proposed IMM-ARUKF during the time period from 200s to 2000s for the vehicle navigation case.

| Filtering Methods | | Position | |
|---|---|---|---|
| | | Longitude | Latitude |
| Classical UKF | MAE(m) | 6.4535 | 6.6170 |
| | STD(m) | 7.9491 | 7.9725 |
| AFUKF | MAE(m) | 4.8049 | 5.4617 |
| | STD(m) | 5.8024 | 6.6258 |
| RUKF | MAE(m) | 4.9728 | 4.4751 |
| | STD(m) | 5.9467 | 5.5518 |
| IMM-ARUKF | MAE(m) | 2.6972 | 2.8339 |
| | STD(m) | 3.2240 | 3.5444 |

The mean absolute errors (MAEs) and standard deviations (STDs) of the position errors by the classical UKF, AFUKF, RUKF and proposed IMM-ARUKF during the time period from 200 s to 2000 s are listed in Table 2. It is evident that the MAE and STD of the position errors by the proposed IMM-ARUKF are also much smaller than those of the other three methods.

The above experiments and analysis confirm that the proposed IMM-ARUKF significantly improves the adaptability and robustness of the classical UKF and overcomes the UKF limitation in the presence of system model uncertainty. It also absorbs the merits and eliminates the limitation of the AFUKF and RUKF, leading to higher estimation accuracy than the classical UKF, AFUKF and RUKF.

## 6. CONCLUSION

This paper presents a novel adaptive robust UKF to address the performance degradation and divergence of the classical UKF in presence of system model uncertainty. The contribution of this paper is that an IMM estimation is developed for fusion of the AFUKF and RUKF to combine their merits and discard their deficiencies, thus inhibiting the disturbance of system model uncertainty. The proposed method establishes an AFUKF for the case of process model uncertainty and a RUKF for the case of measurement model uncertainty. Subsequently, it fuses the above two filters by the IMM estimation as per the mode probability. Based on the above, the overall system state estimation is further obtained as the probabilistic weighted sum of the filtering results from the two filters. Simulation and experimental results as well as comparison analysis demonstrate that the proposed IMM-ARUKF can refrain the disturbances of system model uncertainty on the UKF solution, thus leading to improved filtering adaptability and robustness.

Future research work will focus on the improvement of the proposed IMM-ARUKF. The IMM estimation method

will be combined with the advanced artificial intellegence technologies such as pattern recognition, neural network and advanced expert systems to establish an intelligent algorithm to automatically identify the system mode for fusion of the AFUKF and RUKF.

## REFERENCES


[1] K. Xiong, H. Y. Zhang, and C. W. Chan, "Performance evaluation of UKF-based nonlinear filtering," *Automatica*, vol. 42, no. 2, pp. 261-270, 2006.

[2] Y. Meng, S. S. Gao, Y. M. Zhong, G. G. Hu, and A. Subic, "Covariance matching based adaptive unscented Kalman filter for direct filtering in INS/GNSS integration," *Acta Astronautica*, vol. 120, pp. 171-181, 2016. [click]

[3] W. H. Wei, S. S. Gao, Y. M. Zhong, C. F. Gu, and A. Subic, "Random weighting estimation for systematic error of observation model in dynamic vehicle navigation," *International Journal of Control, Automation and Systems*, vol. 14, no. 2, pp. 514-523, 2016. [click]

[4] Y. Shi and C. Z. Han, "Adaptive UKF method with applications to target tracking," *Acta Automatica Sinica*, vol. 37, no. 6, pp. 755-759, 2011.

[5] W. Wang, Z. Y. Liu, and R. R. Xie, "Quadratic extended Kalman ?lter approach for GPS/INS integration," *Aerospace Science and Technology*, vol. 10, no. 8, pp. 709-713, 2006.

[6] P. S. Pratama, A. V. Gulakari, Y. D. Setiawan, D. H. Kim, H. K. Kim, and S. B. Kim, "Trajectory tracking and fault detection algorithm for automatic guided vehicle based on multiple positioning modules," *International Journal of Control, Automation and Systems*, vol. 14, no. 2, pp. 400-410, 2016. [click]

[7] S. J. Julier and J. K. Uhlmann, "Unscented filtering and nonlinear estimation," *Proceedings of the IEEE*, vol. 92, no. 3, pp. 401-422, 2004. [click]

[8] S. S. Gao, G. G. Hu, and Y. M. Zhong, "Windowing and random weighting-based adaptive unscented Kalman filter," *International Journal of Adaptive Control and Signal Processing*, vol. 29, no. 2, pp. 201-223, 2015. [click]

[9] G. G. Hu, S. S. Gao, Y. M. Zhong, and B. B. Gao, "Stochastic stability of the derivative unscented Kalman filter," *Chinese Physics B*, vol. 24, no. 7, pp. 070202, 2015.

[10] G. G. Hu, S. S. Gao, and Y. M. Zhong, "A derivative UKF for tightly coupled INS/GPS integrated navigation," *ISA transactions*, vol. 56, pp.135-144, 2015. [click]

[11] L. Wang and X. H. Cheng, "Algorithm of Gaussian Sum Filter based on High-order UKF for Dynamic State Estimation," *International Journal of Control, Automation and Systems*, vol. 13, no. 3, pp. 652-661, 2015. [click]

[12] K. Xiong, L. D. Liu, and H. Y. Zhang, "Modified unscented Kalman filtering and its application in autonomous satellite navigation," *Aerospace Science and Technology*, vol. 13, no. 4, pp. 238-246, 2009. [click]

[13] Y. Zhao, S. S. Gao, J. Zhang, and Q. N. Sun, "Robust predictive augmented unscented Kalman filter," *International Journal of Control, Automation and Systems*, vol. 12, no. 5, pp. 996-1004, 2014. [click]

[14] H. E. Soken and C. Hajiyev, "Adaptive fading UKF with Q-adaptation: application to picosatellite attitude estimation," *Journal of Aerospace Engineering*, vol. 26, no. 3, pp. 628-636, 2011.

[15] G. G. Hu, S. S. Gao, Y. M. Zhong, B. B. Gao, and A. Subic, "Modified strong tracking unscented Kalman filter for nonlinear state estimation with process model uncertainty," *International Journal of Adaptive Control and Signal Processing*, vol. 29, no. 12, pp. 1561-1577, 2015. [click]

[16] S. Y. Cho and B. D. Kim, "Adaptive IIR/FIR fusion filter and its application to the INS/GPS integrated system," *Automatica*, vol. 44, no. 8, pp. 2040-2047, 2008. [click]

[17] S. Y. Cho and W. S. Choi. "Robust positioning technique in low-cost DR/GPS for land navigation," *IEEE Transactions on Instrumentation and Measurement*, vol. 55, no. 4, pp. 1132-1142, 2006. [click]

[18] L. Zhao, X. X. Wang, M. Sun, J. C. Ding, and C. Yan, "Adaptive UKF filtering algorithm based on maximum a posterior estimation and exponential weighting," *Acta Automatica Sinica*, vol. 36, no. 7, pp. 1007-1019, 2010.

[19] Q. Song and J. D. Han, "An adaptive UKF algorithm for the state and parameter estimation of a mobile robot," *Acta Automatica Sinica*, vol. 34, no. 1, pp. 72-79, 2008.

[20] D. J. Jwo and F. C. Chung. "Fuzzy Adaptive Unscented Kalman Filter for Ultra-Tight GPS/INS Integration," *Proc. of IEEE International Symposium on Computational Intelligence and Design (ISCID)*, pp. 229-235, 2010. [click]

[21] D. J. Jwo, C. F. Yang, C. H. Chuang, and T. Y. Lee, "Performance enhancement for ultra-tight GPS/INS integration using a fuzzy adaptive strong tracking unscented Kalman filter," *Nonlinear Dynamics*, vol. 73, no. 1-2, pp. 377-395, 2013. [click]

[22] H. E. Soken and C. Hajiyev. "Pico satellite attitude estimation via robust unscented Kalman filter in the presence of measurement faults," *ISA Transactions* vol. 49, no. 3, pp. 249-256, 2010.

[23] L. B. Chang, B. Q. Hu, G. B. Chang, and A. Li, "Huber-based novel robust unscented Kalman filter," *IET Science Measurement Technology*, vol. 6, no. 6, pp. 502-509, 2012. [click]

[24] G. B. Chang, "Kalman filter with both adaptivity and robustness," *Journal of Process Control*, vol. 24, no. 3, pp. 81-87, 2014. [click]

[25] L. A. Johnston and V. Krishnamurthy, "An improvement to the interacting multiple model (IMM) algorithm," *IEEE Transactions on Signal Processing*, vol. 49, no. 12, pp. 2909-2923, 2001. [click]

[26] H. S. Kim, J. G. Park, and D. Lee, "Adaptive fuzzy IMM algorithm for uncertain target tracking," *International Journal of Control, Automation and Systems*, vol. 7, no. 6, pp. 1001-1008, 2009. [click]

[27] C. E. Seah and I. Hwang, "Algorithm for performance analysis of the IMM algorithm," *IEEE Transactions on Aerospace and Electronic Systems*, vol. 47, no. 2, pp. 1114-1124, 2011. [click]

[28] C. E. Seah and I. Hwang, "State estimation for stochastic linear hybrid systems with continuous-state-dependent transitions: an IMM approach," *IEEE Transactions on Aerospace and Electronic Systems*, vol. 45, no. 1, pp. 376-392, 2009. [click]

[29] D. J. Jwo and T. P. Weng, "An adaptive sensor fusion method with applications in integrated navigation," *Journal of Navigation*, vol. 61, no. 4, pp. 705-721, 2008. [click]

[30] D. H. Zhou, Y. X. Su, Y. G. Xi, and Z. J. Zhang, "Extension of Friedland's separate-bias estimation to randomly time-varying bias of nonlinear systems," *IEEE Transactions on Automatic Control*, vol. 38, no. 8, pp. 1270-1273, 1993. [click]

[31] D. H. Zhou, Y. G. Xi, and Z. J. Zhang, "A suboptimal multiple fading extended Kalman filter," *Acta Automatica Sinica*, vol. 17, no. 6, pp. 689-695, 1991.

[32] D. Y. Kim and M. Jeon, "Square Root Receding Horizon Information Filters for Nonlinear Dynamic System Models," *IEEE Transactions on Automatic Control*, vol. 58, no. 5, pp. 1284-1289, 2013. [click]

[33] N. J. Gordon, D. J. Salmond, and A. F. Smith, "Novel approach to nonlinear/non-Gaussian Bayesian state estimation," *IEE Proceedings-F*, vol. 140, no. 2, pp. 107-113, 1993. [click]

[34] B. B. Gao, S. S. Gao, G. G. Hu, and H. F. Yan, "Adaptive UKF based on maximum likelihood principle and receding horizon estimation," *Systems Engineering and Electronics*, vol. 38, no. 7, pp. 1629-1637, 2016.

**Bingbing Gao** is a PhD student at the School of Automatics, Northwestern Polytechnical University, China. His research interests include information fusion, nonlinear filtering and integrated navigation.

**Shesheng Gao** is a Professor at the School of Automatics, Northwestern Polytechnical University, China. His research interests include control theory and engineering, navigation, guidance and control, and information fusion.

**Yongmin Zhong** is an Associate Professor in the School of Engineering at RMIT University. His research interests include computational engineering, virtual reality, haptics, soft tissue modelling and surgery simulation, aerospace navigation and control, intelligent systems and robotics.

**Gaoge Hu** received the D.S. degree in control theory and control engineering from Northwestern Polytechnical University in 2016. His research interests include information fusion, nonlinear filtering and integrated navigation.

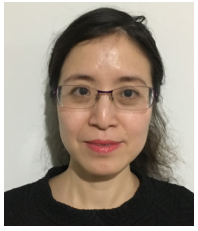

**Chengfan Gu** is a lecturer in the School of Engineering at RMIT University, Australia. Prior to this, she was an ARC DECRA Fellow with UNSW Australia. Her research interests include bio/nano materials characterization and analysis, materials processing, computational modelling and optimization analysis.